CHAPTER 1

MATHEMATICAL MODELING OF INFORMATION PROCESSES IN NEUROPHYSIOLOGY

A MECHANICAL COUPLING MODEL FOR THE AXOLOTL (*Ambystoma tigrinum*) SEMICIRCULAR CANALS

E. Soto[1], V. V. Alexandrov[2], T. B. Alexandrova[2], R. Cruz[1], R. Vega[1], and T. G. Astakhova[2]

We introduce a model of semicircular canals such that the cupula is modeled both as a piston or as a diaphragm. A semicircular canal is modeled as a toroid with the two main components: i) a duct and ii) a widening that forms the ampulla and the utricle. The endolymph motion was described by the Navier–Stokes equations. Our analysis of the model demonstrates that the dynamics of cupular behavior under periodic stimulations is the same in both the piston and diaphragm models. Based on these results, we developed a general model in which the consideration of the detailed cupular structure is not essential. By combining mathematical methods with the morphological analysis of the semicircular canals of the axolotl (*Ambystoma tigrinum*), a system of differential equations describing the cupular displacements as a function of angular acceleration was obtained. The coefficients of this system have an explicit physiological meaning allowing us to introduce morphological and dynamical parameters directly into the differential equations.

---

1. Introduction. The processing of sensory information in the semicircular canals (SCs) of the vestibular system becomes possible due to a diversity of structural and functional components in the sensory periphery. One of these processes is the mechanical coupling between angular accelerations and the motion of the sensory cell hair bundles. This mechanical coupling largely determines the type of mechanical stimuli that might be responsible for the hair cell activation. The properties of mechanical coupling enable the utricle and saccule to function as linear acceleration detectors and the SCs as angular acceleration detectors (even though the above sensory organs are based on sensory cells of a very similar type).

Mathematical modeling of the SCs is essentially based on the fundamental work of Steinhausen [23], who proposed a torsion pendulum model to study the dynamics of the cupula–endolymph system [18, 28], using a linear approach. The model parameters are not strictly related to morphological measurements of the SCs, thus constituting a general model but with poor predictability for particular systems. Further developments of SC models were conducted in the two main directions: i) improvement of the torsion pendulum model proposed by Steinhausen and ii) elaboration of hydrodynamic models of the cupula–endolymph system.

The hydrodynamics of the SCs was first analyzed by Van Buzkirk [27], who modeled the cupula as an elastic weightless membrane that spans the whole ampulla in the form of a diaphragm. Important results were also obtained by Rabbit and Damiano [19]. These authors developed the most detailed dynamic mathematical model of the cupula–endolymph system, simulating the cupula as a diaphragm. Other models considered the cupula as a weighable elastic piston immersed in an ideal liquid [7, 15]. These models have also considered the influence of varying SC shapes on the dynamics of the cupula–endolymph systems.

A combination of pendulum models and hydrodynamic analysis of the cupula–endolymph systems was used in [1, 4] to model such a system as an elastic piston (cupula) immersed in a viscous fluid (endolymph). This allowed the authors to express the coefficients of equations as nonlinear functions of morphological parameters of a particular SC system.

Here we summarize the derivation of the system of differential equations previously presented in an expanded form in [2, 3, 5] and combine this mathematical model with a set of morphological data obtained as a result

[1] Instituto de Fisiología, Universidad Autónoma de Puebla, Apartado Postal 406, Puebla, Pue. 72000, México, e-mail: esoto@siu.buap.mx

[2] Faculty of Mechanics and Mathematics, Moscow State University, Moscow, 119899, Russian Federation, e-mail: valex@moids.math.msu.ru

of our studies of the axolotl inner ear. The results of our theoretical analysis of the cupula modeled either as a diaphragm or as a piston differ little from each other when the system is subjected to periodic stimulations. On this basis a single Steinhausen-type model of the cupula–endolymph system is proposed. The advantage of this model is that it takes into account an explicit dependence of the model coefficients on physiological and morphological parameters.

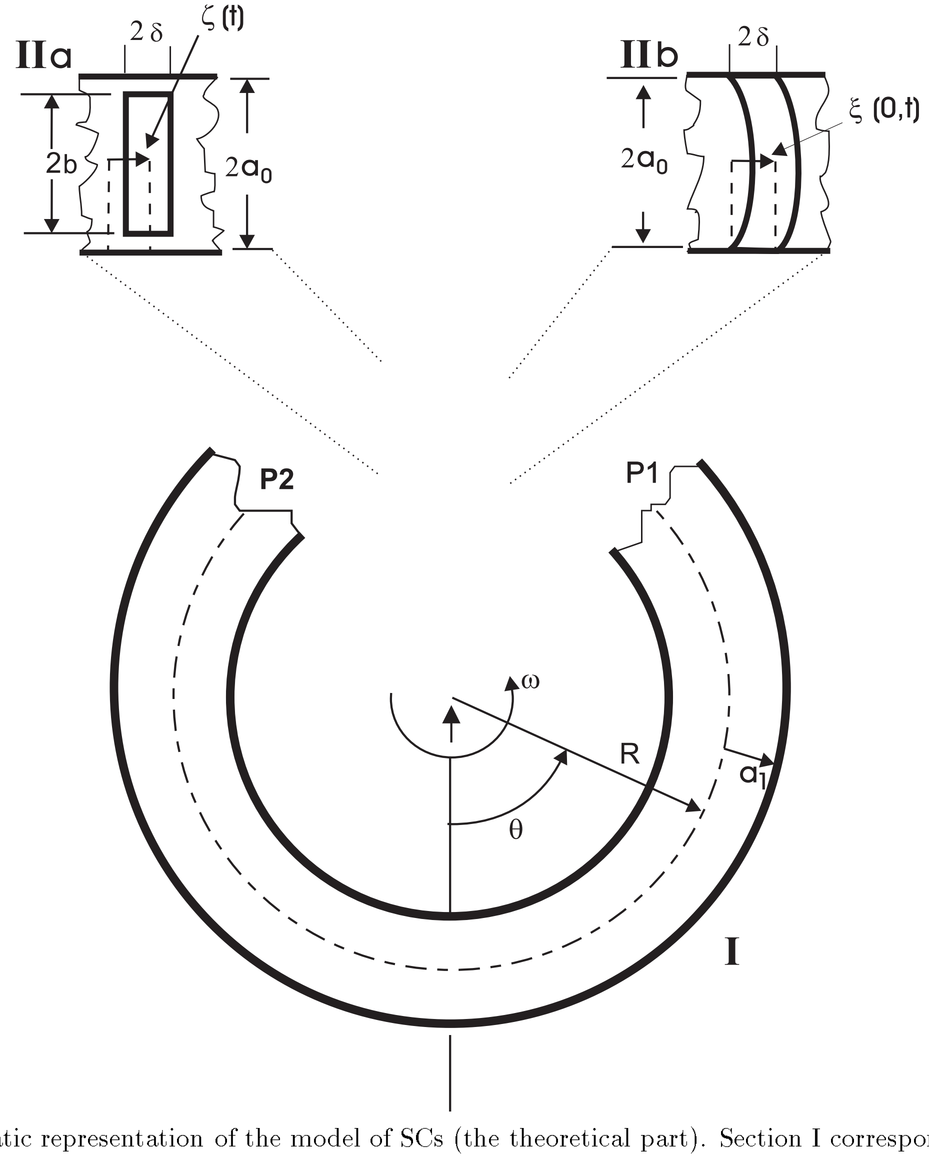

Fig. 1. Schematic representation of the model of SCs (the theoretical part). Section I corresponds to the SC with outer radius R, inner radius a_1, and length L. Sections II a and II b represent the two variants of the cupular structure: the cupula as an elastic piston in the form of a cylinder of width 2δ and diameter $2b$ (shown in II, a) and the cupula as an elastic diaphragm of width 2δ and diameter $2b$ (shown in II, b). In both cases, the canal rotates with the angular velocity ω. $P_1 - P_2$ is the pressure drop between the sides of the cupula

2. Mathematical modeling. The SCs are modeled as toroids opened at their ends to the utricle and filled with a viscous fluid (Figure 1). At one of the ends of each SC, there is a widening that forms the ampulla. The crista ampullaris, where the sensory cells are located, is found in the middle of the ampulla, and the cupula is situated above the crista ampullaris. The sensory cell hair bundles are tightly attached to the cupula. Some controversy exists in regarding the cupula structure. Various models have been proposed to describe the cupula displacements and the attachment to the ampullary walls and to the crista ampullaris [8, 12, 21, 17, 23]. Actually, the diaphragm- and piston-like models of the cupula remain as the most plausible [4, 12, 21].

It is shown in this paper that the cupula can be modeled either as a movable piston or as a diaphragm. These are theoretical-mechanical models that allow taking into account the main forces which define the cupular dynamics.

The various cupula–endolymph models use a similar approach to the description of the endolymph dynamics in the SCs. Based on some mathematical simplifications regarding the endolymph dynamics in a toroidal system described thoroughly in our previous works [2–5], a general description of this system is given by the equation

$$\begin{aligned} &\frac{\partial u}{\partial t} + \dot{\omega} R = -\frac{1}{\rho}\frac{\partial P}{\partial S} + \nu\left(\frac{\partial^2 u}{\partial r^2} + \frac{1}{r}\frac{\partial u}{\partial r}\right) \\ &-\frac{1}{\rho}\frac{\partial P}{\partial S} = \begin{cases} f(t), & |S| \ll R \\ 0, & |S| > R \end{cases} \end{aligned} \tag{1}$$

with the corresponding initial and boundary conditions. Here $\dot{\omega} = \dot{\omega}(t)$ is the absolute angular acceleration of the SC; $u = u(r,t)$ is the longitudinal component of the endolymph velocity relative to the SC walls; r is the inner radius of the duct ($0 \leqslant r \leqslant a_1$); R is the radius of curvature of the SC; S is the longitudinal coordinate measured from the cupula; $dS = R\,d\theta$; $P = P(S,t)$ is the pressure; ν is the kinematic viscosity of the endolymph.

The differential equations used to describe the cupular dynamics depend on the theoretical-mechanical model under consideration. We analyze here two theoretical models of the cupula–endolymph dynamics [3, 4].

2.1. Model of the cupula as a diaphragm. If the cupula is considered as an elastic diaphragm with density ρ, width 2δ, and stiffness T (the cupula is attached to the ampulla of diameter $2a_0$ ($a_0 > a_1$) that completely blocks the endolymph flux), then the displacement $\xi(r,t)$ of the cupula relative to the equilibrium point (Figure 1, IIb) is perpendicular to its equilibrium plane and is described by

$$\begin{aligned} &2\delta\rho\left(\ddot{\xi} + \dot{\omega} R\right) = T\nabla^2\xi + (P_1 - P_2) \\ &\xi(a_0,t) = 0, \qquad \partial\xi(0;t)/\partial r = 0 \end{aligned} \tag{2}$$

The pressure drop $P_1 - P_2$ at the cupular level is specified by the endolymph dynamics in the canal, as described by equation (1) with the corresponding initial conditions and the following boundary conditions:

$u(a_1,t) = 0$ at the vestibular canal walls,

$u(r,t) = \dot{\xi}(r,t)$ at the cupular level, $0 \leqslant r \leqslant a_0$.

In this case, equations (1) and (2) describe the dynamics of the cupula–endolymph system when the cupula has the form of a diaphragm.

2.2. Model of the cupula as a piston. If the cupula structure is thought of as a mobile piston with density ρ, width 2δ, and height $2b$, then between the piston and the ampullary wall there is a cleft through which the endolymph can flow. The manner by which the piston is attached to the ampullary wall is not analyzed here. It is assumed that as the piston moves, there appear elastic forces proportional to the piston displacement.

The balance between the inertial forces, pressure difference at both sides of the piston, elastic forces of the piston, and the frictional forces at the lateral walls of the piston will determine the motion of the piston in the canal:

$$m_0\left(\ddot{\zeta} + \dot{\omega} R\right) = \int_0^b \int_0^{2\pi} (P_1 - P_2)\, r\, dr\, d\varphi - F_T - \gamma\zeta \tag{3}$$

Here m_0 is the mass of the piston, ζ is its displacement relative to the equilibrium point (when $\dot{\omega} = 0$), $P_1 - P_2$ is the pressure drop between the sides of the cupula, F_T is the frictional viscous force at the lateral wall of the piston, and γ is the elastic force coefficient that appears during the motion of the piston. In order to determine $F(t)$, an approximate variant of equation (1) derived for a lubricated layer [4] can be used.

The dynamics of the cupula–endolymph system is therefore described by equations (1) and (3) (when the cupula is considered as a piston) with the corresponding initial conditions and the following boundary conditions: $u(a_1,t) = 0$, $u(a_0,t) = 0$, $u(r,t) = \dot{\zeta}(t)$ at the cupula.

Therefore, there are two models of the cupula–endolymph system: one of them described by equations (1) and (2) corresponds to a diaphragm-like cupula and the other model described by equations (1) and (3) corresponds to a piston-like cupula. In the previous paper [2], we have shown that, under periodic mechanical stimulations, these two models gave very similar results. On this basis, using some additional suppositions on the shape of the parabolic profile for the fluid velocity in the SC and using Tikhonov's theory [26] for systems with small parameters [4], a unified approximate model of cupula–endolymph dynamics was obtained according to the following equation:

$$\ddot{x} + \frac{8\nu}{a_1^2}\,\dot{x} + \frac{\gamma}{mk^4}\,x = -\frac{1}{k^2}\left(1 + \frac{l}{L}\right) R\dot{\omega} \tag{4}$$

Here $k = a_0/a_1 > 1$ is the expansion coefficient, m is the endolymph mass in the SC of length L, l is the utricle length, and x is the relative displacement of the cupula from the equilibrium state. For the piston-like model this displacement takes the form $\zeta = x$, whereas for the diaphragm-like model it is expressed by

$$\xi(r,t) = 2x(t)\left(1 - \frac{r^2}{a_0^2}\right), \quad 0 \leqslant r \leqslant a_0, \quad \gamma = 8\pi T$$

where T is the stiffness of the membrane.

In the case when the cupula is modeled as a piston, the existence of a cleft between the cupula and the SC walls originates an additional dissipative force equal to

$$\frac{8\bar{\nu}}{a_1^2}\left[\frac{\delta a_0}{2l(a_0 - b)k^4}\right]\dot{x} \tag{5}$$

This expression is negligible, since

$$\frac{\delta a_0}{2l(a_0 - b)k^4} \ll 1 \tag{6}$$

Using the kinematic model of the mutual influence effects of SCs developed in [22], an approximate model of a finite dimension for the cupula–endolymph system with three SCs can be written ($i = 1, 2, 3$):

$$\ddot{x}_i + \frac{8\nu}{a_{1i}^2}\,\dot{x}_i + \frac{\gamma_i}{m_i k_i^4}\,x_i + \sum_{j=1}^{3}\lambda_{ij}\dot{x}_j = -\frac{R_i\dot{\omega}_i}{k_i^2}\left(1 + \frac{l_i}{L_i}\right) \tag{7}$$

Here λ_{ij} are the coefficients of mutual influence effects and a_{1i} is the corresponding duct radius. Due to the fact that the anterior and posterior SCs have a part in common, the flow of endolymph in each of these canals influences the response of the other one. It has also been shown that the endolymph flow in the lateral canal may influence responses of both the anterior and posterior canals [22]. Since in the axolotl there is also a common segment in the anterior and lateral canals, the endolymph flow in one of these canals will influence the response of the other. As a consequence of the fact that five of the interaction coefficients (their total number is nine) are not equal to zero (the SCs are numbered as: anterior 1, posterior 2, and lateral 3), we have $\lambda_{12} \neq 0$, $\lambda_{13} \neq 0$, $\lambda_{21} \neq 0$, $\lambda_{23} \neq 0$, $\lambda_{31} \neq 0$, $\lambda_{11} = \lambda_{22} = \lambda_{33} = \lambda_{32} = 0$. In addition, $\lambda_{13}\lambda_{23} < 0$ and $\lambda_{12} > 0$, $\lambda_{21} > 0$ [4, 22]. The parameters a_j, R_j, k_j, l_j, and L_j can be called as anatomical and the parameters ν, γ_i, λ_{12}, λ_{13}, λ_{21}, λ_{23}, and λ_{31} as dynamical.

The main advantage of the model summarized here is that the coefficients are known functions of the dynamical and anatomical parameters for the SCs. In this case, equation (7) constitutes a general approximate model of the cupula–endolymph system in the SCs. This model can be combined with measurements of the SCs morphology to define parameters and account for particular cases.

3. Material and methods. Larval axolotls (*Ambystoma tigrinum*) of about 60 g in weight each were anesthetized with 3 aminobenzoic acid ethyl ester methasulfonate (MS-222) 0.1%. After 10 min, the animals were decapitated and the lower jaws were cut. The roof of the mouth of each axolotl was dissected and the otic capsule was opened. Drops of a fixing solution were placed in the otic capsule and the whole animal head was immersed in the cool (4° C) fixing solution for the further isolation of the inner ear. The fixing solution was made of glutaraldeheide 2 % or osmium 2 % in 0.1 phosphate buffer pH adjusted to 7.4 [9, 11]. Osmolarity of this solution was always 240 mOsm. When needed, sucrose was added to reach the optimal osmolarity value. The animal housing and the experimental procedures were performed according to the guidelines of the declaration of Helsinki.

After fixation, the whole inner ear and its organs were inspected by stereomicroscopic observation and with the use of rapid photographic processing [10]. In addition, osmium fixed preparations were placed in petri dishes containing phosphate buffer 0.1 mM and photographed by a stereomicroscope. For decalcification, the tissue was treated in a solution containing 1 % nitric acid and 0.1 % formaldehyde for 24 hours.

3.1. Optical microscopy. For the optical microscopy analysis, the inner ear was dissected, the utricle, saccule, lagena, and SCs were isolated. Preparations were dehydrated and embedded in Spurr or Durcupan ACM synthetic resins.

The tissue pieces were cut in a manual Porter–Blum ultramicrotome (Dupont, MT-1), using glass knives. The resulting tissue sections of 1 – 2 μm in thickness were placed on gelatinized slides and stained with toluidine blue 1 % for 5 – 10 min. Then, these tissue sections were rinsed, dried overnight, and dehydrated in an ethanol series. Finally, they were dried, embedded in synthetic resin, analyzed with a light microscope (Zeiss Axioplan), and photographed with Kodak Ektachrome 100 and Tmax 100 film.

3.2. Scanning electron microscopy. The tissue was fixed either with Karnowsky's fixative or with 2 % osmium solution. Then, the inner ear was treated by the OTOTO technique as follows: the tissue pieces were first immersed in a saturated solution of thiocarbohydrazide (20 min) and then in a 1 % osmium aqueous solution (2 hr). This procedure was repeated twice, washing the preparations thoroughly. After rinsing in the phosphate buffer solution, the preparations were carefully dissected in 70 % alcohol. A jet of alcohol ejected gently from a pipette removed the otolith. The preparations were dehydrated in a graded ethanol series and dryed by the critical point method, using carbon dioxide.

Shortly before the examination, some of the preparations were covered with a nanometric silver film and observed in a Jeol (JSV-5400-LV) scanning electron microscope with a voltage between 10 and 30 KV [25].

3.3. Morphometric analysis. Micrographs were analyzed by the use of a digitizing tablet (Calcomp) and ad hoc software. Digital images were arranged and printed using Adobe Photoshop 4.0$^{\mathrm{TM}}$. To measure circular structures such as the semicircular canal, we always took the size of the smallest of the diameters. The dimensions of the SC crista were measured directly from the scanning electron and optical microscope micrographs. No corrections for curvature or fixation-induced shrinkage was applied. To calculate the volume of the endolymph in the SC ampulla, it was assumed that ampullae have the form of an American football ball with their tips cut away. The volume of this structure is determined by obtaining data on its three dimensions: the ampulla length, width, and height ($2a_0$). The ampulla width is equal to the crista length (see Table I).

Table I. The semicircular canal morphological parameters (data in mm)

	Anterior			Lateral			Posterior		
	N	Mean	SD	N	Mean	SD	N	Mean	SD
SC length	9	3.3	0.35	8	4.6	0.35	10	2.8	0.27
SC Diameter: $2a_1$	11	0.30	0.03	13	0.31	0.03	10	0.31	0.02
SC Radius: R	9	0.93	0.06	8	1.35	0.06	10	0.89	0.04
Ampulla length	8	0.79	0.04	9	0.92	0.08	9	0.96	0.05
Ampulla height: $2a_0$	7	0.58	0.04	3	0.71	0.04	6	0.68	0.04
Cupula height	6	0.41	0.01	7	0.55	0.06	9	0.44	0.05
Crista height	5	0.20	0.01	3	0.21	0.008	6	0.22	0.01
Crista thickness: 2δ	3	0.16	0.01	4	0.15	0.02	5	0.13	0.02
Crista length	9	0.56	0.04	12	0.64	0.03	12	0.59	0.05
Utricle fraction*	9	2.78	0.20	7	2.92	0.10	9	1.80	0.10

* The utricle fraction is the segment of the SC circuit formed by the utricle

4. Results.

4.1. Morphology. The anterior and lateral canals are of ellipsoidal shape with their maximum radii of 0.93 and 1.35 mm, respectively, whereas the posterior canal is of quasicircular shape with a radius of 0.89 mm. The duct radius 150 μm was nearly the same in the three canals.

The SC ampullae were identified as an enlargement of the SC duct (Figure 2, A). The morphological measurements obtained from three ampullae are shown in Table I. The lateral canal ampulla turned out to be the largest one (its volume is 1.68 times larger than that of the anterior canal and 1.18 times larger than that of the posterior canal). This volume is larger mainly because of the fact that the lateral canal ampulla has a larger cupular space, its cupula is 1.24 and 1.34 times higher than that of the posterior and anterior canals, respectively (Table I). The utricle opening of the lateral canal ampulla is 2.38 and 1.62 times wider than that of the posterior and anterior canals, respectively.

The anterior and posterior SC cristae are both symmetric, showing a central enlargement. They have about 450 hair cells each. The lateral canal crista was found to be nonsymmetric, increasing in its cross section towards the external side of the SC (Figures 2, B and C). It showed no central enlargement and had about 550

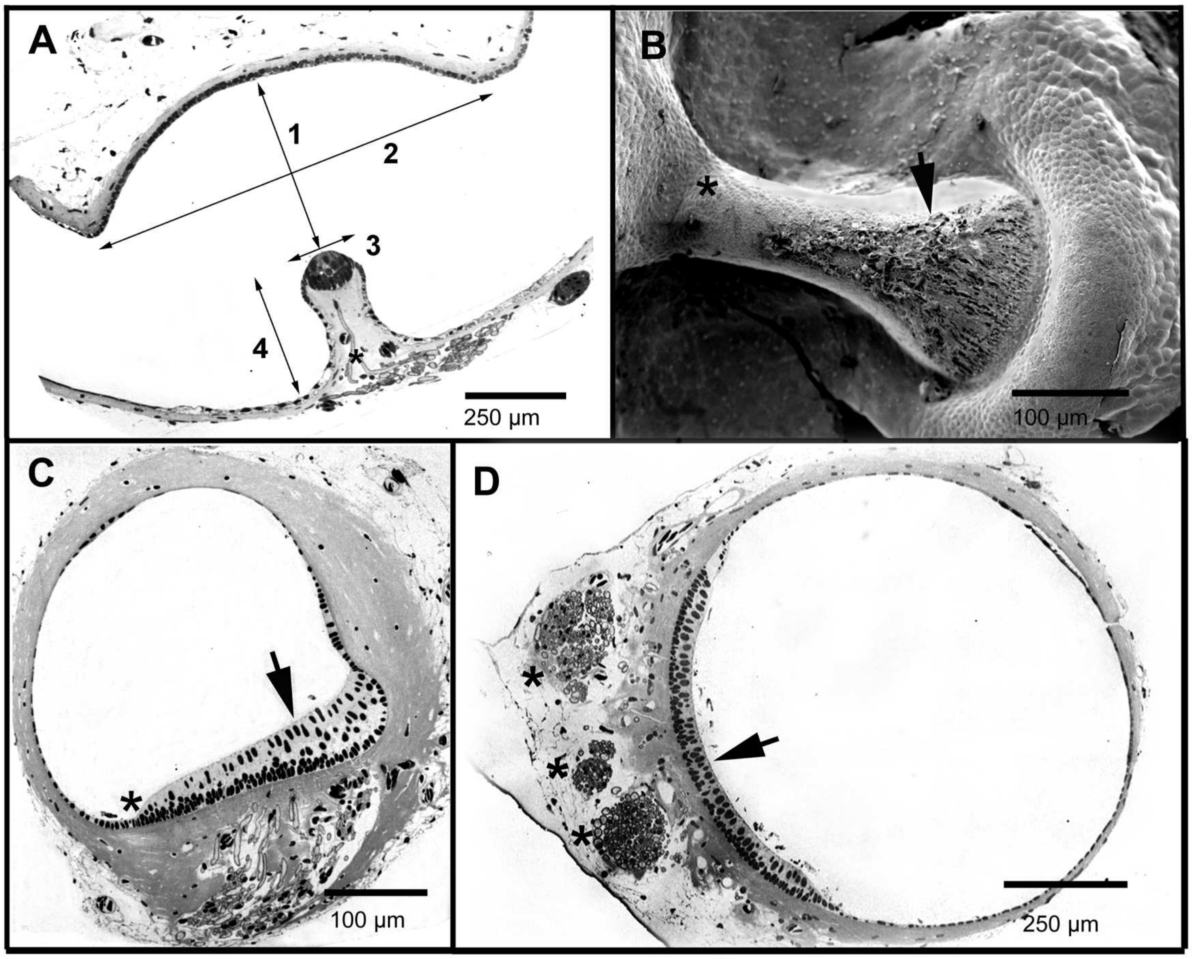

Fig. 2. Optical and scanning electron micrographs of the axolotl inner ear. A: the tissue section of the posterior SC ampulla. The ampulla is delimited by the narrowing of the SC. The crista ampullaris is located in the midst of the ampulla. This figure shows the measurements: 1 — ampulla height ($2a_0$), 2 — ampulla length, 3 — crista thickness (2δ), 4 — crista height. The mielinated axons innervating the crista hair cells are identifiable (*). B and C: scanning electron microscopy and optical microscopy of the lateral semicircular crista ampullaris. This is a nonsymmetric structure with a large widening at the external wall of the ampulla (arrowhead), where the hair cells are concentrated, and leaving what seems to be a cleft in the internal side of the ampulla (*). The pictures in B and C are from different animals. D: cross section of the utricle. The macula (arrowhead) is located ventrally and occupies about a third of its perimeter. The mielinated axons innervating the macula hair cells are located below the neuroepithelia forming three rami (*)

hair cells [6]. It is worth noting that the lateral canal crista is 3.33 thicker than the anterior and posterior canal cristae (Tables I and II); this probably means a completely different cupular elasticity.

Differences in the position of the ampullary crista are worth noting. The crista ampullaris of the posterior and anterior SCs are positioned at the outer arch of the ampulla wall with the cupula extending from the crista across the ampulla to the inner arch. The crista of the lateral canal is positioned at the inner arch of the circuit with the cupula extending to the outer arch. With the use of the scanning electron microscopy, we have searched for evidences of the attachment of the cupula to the lateral walls of the ampulla. Except for a faint signal in the external wall of the lateral canal ampulla (see Figure 2, B), no evidence of the cupular attachment to the lateral wall of the ampulla was found.

The utricle is a cylindrical organ with a quasicircular cross section (Figure 2, D). The utricle length (l) is 3.16 ± 0.13 mm ($n = 9$) and its maximum diameter is 0.79 ± 0.11 mm ($n = 7$). The sensorial macula is positioned in the ventral side of the utricle. The contribution of the utricle to the SC circuits (distinguished in

Table II. The anatomical parameters* of the mathematical model for the semicircular canals of the axolotl

	Anterior	Lateral	Posterior
$2a_1$	0.3 mm	0.31 mm	0.31 mm
k	1.9	2.3	2.2
R	0.93 mm	1.35 mm	0.89 mm
L	3.3 mm	4.6 mm	2.8 mm
l^{**}	3.57 mm	3.84 mm	2.76 mm
m	3.1 mg	4.5 mg	2.7 mg

* By anatomical parameters we mean those that were calculated and by morphological ones those that were measured directly in the histological specimen.
** l is the sum of utricle fraction (see Table I) plus the ampulla length.

Table I as the utricle fraction) varies for the three SCs. The utricle forms 32 % of the anterior SC circuit, 47.2 % of the lateral canal, and 32 % of the posterior canal. It is not clear to which extent the endolymph mass in the utricle influences the overall response of the system; however, our results imply that the effective endolymph mass in the lateral canal is probably larger than that found in the posterior and anterior canals. In the axolotl, the anterior and lateral SC openings in the ampullary side of the duct form a ridge dividing the utricle into two halves. This suggests that there may exist significant mutual effects between these two canals.

4.2. Mathematical model. The morphological parameters (Table I) can be used to calculate the anatomical parameters of the model (Table II). Mathematical model (7) with morphological parameters for the dynamics of the SCs can be written as follows:

$$\begin{aligned}
&\ddot{x}_1 + \frac{8\nu}{0.09}\,\dot{x}_1 + \frac{\gamma_1}{39}\,x_1 + \lambda_{12}\,\dot{x}_2 + \lambda_{13}\,\dot{x}_3 = -0.54\,\dot{\omega}_1\\
&\ddot{x}_2 + \frac{8\nu}{0.096}\,\dot{x}_2 + \frac{\gamma_2}{63}\,x_2 + \lambda_{21}\,\dot{x}_1 + \lambda_{23}\,\dot{x}_3 = -0.36\,\dot{\omega}_2\\
&\ddot{x}_3 + \frac{8\nu}{0.09}\,\dot{x}_3 + \frac{\gamma_3}{126}\,x_3 + \lambda_{31}\,\dot{x}_1 = -0.45\,\dot{\omega}_3
\end{aligned} \tag{8}$$

The coefficients that appear in mathematical model (8) were obtained from the mean values given in Table I. It is worth noting that there are different parameters, which characterize the elasticity of the cupula (γ_i) in model (8) because of the differences in the morphology of the SC crista among the three canals.

In this model, the number of dynamical parameters involved is equal to nine: ν, γ_1, γ_2, γ_3, $\lambda_{12} > 0$, $\lambda_{21} > 0$, λ_{13}, λ_{23} ($\lambda_{13}\lambda_{23} < 0$), λ_{31}. For the identification of these parameters, it is necessary to perform some dynamical experiments. The number of experiments needed for this identification must be determined on the basis of the confidence intervals corresponding to the mean quadratic deviations given in Table I.

According to the statistical data given in Table I, we can come to the conclusion that a cleft of 0.02 μm in height is situated in the posterior canal (cleft height = ampulla height − cupula height − crista height; hence, $a_0 - b = 0.01$. Then, using data from Tables I and II ($\delta = 0.06$ mm, $a_0 = 0.34$, $L = 2.8$ mm, $k = 2.2$), we conclude that inequality (6) is valid: $0.015 \ll 1$. It is clear from this example that for our mathematical model the question on the existence of a cleft in the cupula is of little importance.

We assume that the viscosity of the endolymph is close to that reported for humans: $\nu = 0.8$ mm^2/sec [22] (for the exactness of calculations, it should be taken into account that viscosity of the endolymph depends on temperature; hence, it is very probable that axolotl endolymph viscosity could be greater). The elastic force coefficient γ is estimated as $\gamma \in [0.05$ g/sec^2; 0.2 g/sec$^2]$ [1]. Therefore, $\gamma/mk^2 < 10$ and, for the small time constant τ, we obtain

$$\tau_i \simeq \frac{a_{1i}^2}{8\nu} \approx 0.003 \text{ sec}, \quad i = 1, 2, 3$$

This result is in agreement with similar calculations obtained previously [28].

For the identification of the large time constants T_1, T_2, and T_3, it is necessary to identify the mutual influence coefficients of the anterior, lateral, and posterior canals λ_{12}, λ_{21}, λ_{23}, λ_{13}, λ_{31} and the coefficients of elasticity γ_1, γ_2, and γ_3 for the corresponding cupulae.

As a consequence of the above, it is possible to design dynamical experiments that allow us to determine the dynamical parameters of the model, as has been done previously for the Steinhausen model [20]. For example, in the case of the model described by equation (8), morphological measurements permit identifying R, k, a_1, and m. Thus, ν, γ_i, λ_{12}, λ_{21}, λ_{13}, λ_{23}, λ_{31} may be identified by dynamical experiments.

5. Discussion. The main advantage of the model presented here is that the coefficients of the model are known functions of morphological and dynamical parameters of the SCs. Based on morphological measurements of the SCs, it is possible to incorporate the resulting data directly into the model. In addition, as in the case of Steinhausen-type models, our model (4) – (8) is simpler than those described by partial differential equations or by integro-differential equations.

Recall that the coefficient of expansion k is about 5 for human SCs and is about 2 for the axolotl. From dynamic equation (4) we obtain the static equation

$$\varphi = \frac{k^2 m}{\gamma}\left(1 + \frac{l}{L}\right) R\dot{\omega} \tag{9}$$

Thus, the coefficient of expansion k and the utricle length l increase the displacements of the cupula. Therefore, studies of dynamical processes can be performed on the basis of an analysis of the morphological specificity of SCs. The presence of the utricle in our model leads to an increase of incoming signals, as can be deduced from equation (9). However, the utricle contribution to the lateral and anterior canal circuits is larger than in the posterior canal (see (9)). Note that the choice of geometry of canals (ellipsoidal or circular) should also be considered during the process of mathematical modeling. In our model, we proposed the toroidal shape (with mean radius given in Table I), but it is clear that this is a simplification, since the SC shape is commonly assumed to be ellipsoidal.

Modeling the cupula as a piston admits important simplifications. This is a mathematical abstraction in which no consideration is given to the piston attachment. The system acquires the equilibrium position of the cupula when the static fluid pressure exists. Since the endolymph flow is laminar, the velocity is close to zero near the wall of the canal, whereas the central part of the cupula is subjected to greater deformation, performing a diaphragm-like or piston-like motion. Thus, it is probable that even assuming the existence of a lateral cleft, no macroscopic flow of the endolymph through the cupula will take place; therefore, experiments with dyes intended to demonstrate whether a cleft in the cupula exists could not be sufficient to make this question clear [12]. The exact morphology of the cupula is still under discussion, and there is an evidence suggesting that a cleft (septum cruciatum) exists in posterior SCs of some animals [13]. Light-microscopic observations of the cupula *in-vivo* have also shown that the base of the cupula is at the level of the tips of the cilia. Thus, there is a subcupular space causing the cupula to perform a diaphragm-like or piston-like motion in such a manner that the cupula changes its position only slightly during stimuli [17]. By analogy with the saccule, it is very probable that the subcupular space is filled with a columnar filament layer bridged by the hair bundles of sensory cells [14].

As for a possible endolymph leakage in the cleft between the piston and the ampulla wall, the theoretical mechanical model in the form presented here shows negligible effects of this phenomenon on the dynamics of the cupula endolymph system. The inclusion of the lubrication hydrodynamic layer between the cupula-piston and the ampulla wall introduces an additional viscous damping (5) in equation (4). It is also shown that according to our assumptions the viscous damping can be ignored. On the basis of inequality (6), it can be concluded that the viscosity forces which appear in the cleft between the cupula and the wall of the SC are small if compared with the viscosity forces which appear during the process of motion of the endolymph in the SC. Therefore, we can conclude that the discussion on the existence of an endolymphatic flow through the cupula has no principal significance for mathematical modeling of cupular displacements.

The physiological significance of asymmetries in the crista ampullaris between the lateral canal and the anterior and posterior canals has not been taken into account. Undoubtedly, the structures of the crista ampullaris and the cupula may play an essential role in determining the cupular displacement, although there are evidences suggesting that the elastic element plays a minor role in determining the mechanical behavior of the semicircular duct system [16]. The model presented here also implies the consideration of a more complex configuration including the other two SCs and the coefficient of mutual influence existing among them [22].

The morphological data presented here allow for the identification of the anatomical parameters of the model. In general, our data are in agreement with the previous descriptions of the amphibian inner ear and constitute, to our best knowledge, the first ultrastructural quantification of SCs and the utricular morphology of the axolotl. The relationship between the radius of curvature R and the SC duct radius r can be expressed as follows: $R_{\mathrm{a}} = 6.2 r_{\mathrm{a}}$, $R_{\mathrm{l}} = 8.7 r_{\mathrm{l}}$, and $R_{\mathrm{p}} = 5.8 r_{\mathrm{p}}$; this suggests that the axolotl SCs have a low sensitivity and high frequency of response system as compared with other vertebrates [16].

The model parameters can be divided into the two groups: anatomical and dynamical. The progress in parameter identification is based on the planning of dynamical experiments. Unknown parameters, such as the kinematic viscosity of the endolymph, elasticity coefficient of the cupula and effective viscosity, should be approximated on the basis of analysis of a mathematical model of the cupula–endolymph system. There are two possibilities for the identification of these parameters: the first one is to measure cupula displacements in dynamical experiments and then, by means of identification algorithms, to estimate the unknown parameters. The second possibility is to register the output of the system (activity of SC afferent neurons) in dynamical experiments [24]. In the latter case, the addition of various components to the model is surely needed to account for the processes that take place in the hair cell, the synapse, and the primary afferent neurons.

6. Acknowledgments. The authors wish to thank Professor Augustine Udeh for careful reading of the manuscript. Dr. Rutilo Silva, Carlos Corona and Jorge Guevara are thanked for their invaluable help with the scanning electron microscopy. This research was partially supported by CONACyT grant 35525-N to E.S.

REFERENCES

1. V.V. Alexandrov, T.B. Alexandrova, T.G. Astakhova, and V.A. Sadovnichii, "Mathematical models of physiological systems and dynamic simulations of sensorial conflicts under zero gravity", *Fundamental and Applied mathematics*, 3: 129–147, 1997.
2. V.V. Alexandrov, T.B. Alexandrova, T.G. Astakhova, A.G. Yakushev, and E. Soto, "Equations of the dynamics of the cupula–endolymph system in semicircular canals, *Differential Equations*, 35(4): 1–6, 1999.
3. V.V. Alexandrov, T.G. Astakhova, and T. Trincher, "Mathematical modeling of the dynamics of the cupula–endolymph system", *Moscow Univ. Mech. Bull.*, 5: 72–76, 1999.
4. T.G. Astakhova, "Mathematical model of the semicircular canal of the vestibular system as an angular acceleration sensor", *Moscow Univ. Mech. Bull.*, 1: 69–72, 1989.
5. T.G. Astakhova, *Mathematical Model of the Semicircular Canal of the Vestibular System*, Ph.D. Thesis. Moscow State University, 1990.
6. R. Cruz-Vera, *Patrón de Inervación, Ultraestructura y Biofísica de los Canales Semicirculares en el Axolotl (Ambystoma Mexicanum)*, Tesis de Licenciatura, Escuela de Ciencias Química, Universidad Autónoma de Puebla, México, 1994.
7. I.S. Curthoys and C.M. Oman, "Dimensions of the horizontal semicircular duct, ampulla and utricle in human", *Acta Otolaryngol.*, 103: 254–261, 1987.
8. G.F. Dohlman, "The shape and function of the cupula", *J. Laryngol. Otol.*, 83: 43–53, 1969.
9. M.A. Glauter, *Fixation, Dehydration and Embedding of Biological Specimens: Practical Methods in Electron Microscopy*, New York: Elsevier Sci., 1987.
10. C.M. Guzman-Flores, M. Alcaraz, and A. Fernández-Guardiola, "Procedimiento rápido para localizar electrodos en la neurofisiología experimental", *Bol. Estud. Med. Biol.*, 16: 26–31, 1958.
11. M.A. Hayat, *Basic Techniques for Transmission Electron Microscopy*, Orlando: Academic Press, 1986.
12. D.E. Hillman and J.W. McLaren, "Displacement configuration of semicircular canal cupulae", *Neuroscience*, 4: 1989–2000, 1979.
13. I.M. Hunter-Duvar, "An electron microscopic study of the vestibular sensory epithelium", *Acta Otolaryngol.*, 95: 494–507, 1983.
14. B. Kachar, M. Parakkal, and J. Fex, "Structural basis for mechanical transduction in the frog vestibular sensory apparatus: I. The otolithic membrane", *Hearing Res.*, 45: 179-190, 1990.
15. A.V. Kondrachuk, S.P. Sirenko, and A.A. Shipov, "Mathematical simulation of the gravity receptor", *Physiology*, **34**: S212–S213, 1981
16. M. Muller, "Size limitations in semicircular duct systems", *J. Theor. Biol.*, 198: 405–437, 1999.
17. G. Nagel, D.C. Neugebauer, B. Schmidt, and U. Thurm, "Structures transmitting stimulatory force to the sensory hairs of vestibular ampullae of fishes and frog", *Cell Tissue Res.*, 265: 567–578, 1991.
18. C.M. Oman and I.R. Young, "The physiological range of pressure difference and cupula deflections in the human semicircular canal", *Acta Otolaryngol.*, 74: 324–331, 1972.

19. R.D. Rabbit and E.R. Damiano, "A hydroelastic model of macromechanics in the endolymphatic vestibular canal", *J. Fluid Mechanics*, 238: 337–369, 1992.

20. M.L. Rossi and M. Martini, "Some hydrodynamic properties of the posterior canal in the frog labyrinth related to neuronal responses", *Neurosci. Lett.*, 66: 328–332, 1986.

21. A. Rüsch and U. Thurm, "Cupula displacement, hair bundle deflection, and physiological responses in the transparent semicircular canal of young eel", *European J. Physiol.*, 413: 533–545, 1989.

22. A.A. Shipov, A.V. Kondrachuk, and S.P. Sirenko, *Biomechanics of the Vestibular Apparatus* (in Russian), Moscow, 1997.

23. W. Shteinhausen, "Über die Beobachtung der Cupula in den Bogengangsampullen des Labirinthes des libenden Heechts", *Pflug. Arch.*, 232: 500–512, 1933.

24. E. Soto, A. Flores, C. Eróstegui, and R. Vega, "Evidence for NMDA receptor in the afferent synaptic transmission of the vestibular system", *Brain Res.*, 633: 289–296, 1994.

25. E. Soto, J. Guevara, J. Andrade, and R. Cruz-Vera, "Ultraestructura e inervación del oído interno en el axolotl (*Ambystoma mexicanum*)", in: *Segundo Congreso Mexicano de Microscopía Electrónica. Cancún* (in Spanish), SSB14, 1994.

26. A.B. Vasil'eva and A.G. Sveshnikov, *Differential Equations* (in Russian), Moscow, 1985.

27. W.C. Van Buskirk, "The effect of the utricle on fluid flow in the semicircular canals", *Ann. Biomed. Engin.*, 5: 1–11, 1977.

28. A.J. Van-Egmond, J.J. Groen, and L.B.W. Kongkees, "The mechanics of semicircular canal", *J. Physiol.*, 110: 1–17, 1949.